Direct evidence for RNA–RNA interactions at the 3′ end of the Hepatitis C virus genome using surface plasmon resonance

WILLIAM PALAU,[1,2] CYRIL MASANTE,[3,4] MICHEL VENTURA,[3,4] and CARMELO DI PRIMO[1,2,5]

[1]Université de Bordeaux, Laboratoire ARNA, F-33000 Bordeaux, France
[2]INSERM, U869, Laboratoire ARNA, F-33600 Pessac, France
[3]Université de Bordeaux, Laboratoire MFP-UMR5234, F-33000 Bordeaux, France
[4]CNRS UMR 5234, Laboratoire MFP-UMR5234, F-33000 Bordeaux, France

ABSTRACT

Surface plasmon resonance was used to investigate two previously described interactions analyzed by reverse genetics and complementation mutation experiments, involving 5BSL3.2, a stem–loop located in the NS5B coding region of HCV. 5BSL3.2 was immobilized on a sensor chip by streptavidin-biotin coupling, and its interaction either with the SL2 stem–loop of the 3′ end or with an upstream sequence centered on nucleotide 9110 (referred to as Seq9110) was monitored in real-time. In contrast with previous results obtained by NMR assays with the same short RNA sequences that we used or SHAPE analysis with longer RNAs, we demonstrate that recognition between 5BSL3.2 and SL2 can occur in solution through a kissing-loop interaction. We show that recognition between Seq9110 and the internal loop of 5BSL3.2 does not prevent binding of SL2 on the apical loop of 5BSL3.2 and does not influence the rate constants of the SL2-5BSL3.2 complex. Therefore, the two binding sites of 5BSL3.2, the apical and internal loops, are structurally independent and both interactions can coexist. We finally show that the stem–loop SL2 is a highly dynamic RNA motif that fluctuates between at least two conformations: One is able to hybridize with 5BSL3.2 through loop–loop interaction, and the other one is capable of self-associating in the absence of protein, reinforcing the hypothesis of SL2 being a dimerization sequence. This result suggests also that the conformational dynamics of SL2 could play a crucial role for controlling the destiny of the genomic RNA.

Keywords: Hepatitis C virus; RNA; interactions; kissing loop; kinetics; SPR

INTRODUCTION

The Hepatitis C virus (HCV) is a human viral pathogen of the family of the Flaviridae. The HCV genome is a positive-sense single-stranded RNA that encodes a long open reading frame (ORF). This ORF is translated as a polyprotein of about 3010 amino acids (Clarke 1997). The coding sequence is flanked by two untranslated regions (UTR). The 341-nt 5′ UTR and the first nucleotides encoding the capsid protein form a highly structured domain that serves as an internal ribosome entry site (IRES) initiating the ORF translation in a cap-independent manner. The 3′ UTR is composed of a short variable region, a polyU/C tract of variable length and a 98-nt sequence

(3′X), highly conserved among various isolates (Tanaka et al. 1995), which folds as three contiguous stem–loops, SL1, SL2, and SL3 (Fig. 1A; Friebe and Bartenschlager 2002; Yi and Lemon 2003).

Evidence has now accumulated suggesting that RNA–RNA interactions between structured regions of the HCV genome are crucial to regulate the life cycle of the virus (You et al. 2004; Friebe et al. 2005; Diviney et al. 2008; You and Rice 2008; Tuplin et al. 2012).

Several interactions in the HCV genome involve a structured RNA motif, known as 5BSL3.2, located within the NS5B coding region (Fig. 1A). This imperfect hairpin of 48 nt has been shown to play a role in the life cycle of HCV and would act as a molecular hub capable of interacting with other RNA regions within the viral RNA. 5BSL3.2 displays a 7-nt sequence in an apical loop (Fig. 1B) that would recognize stem–loop SL2, through kissing-loop interactions (You et al. 2004; Friebe et al. 2005; You and Rice 2008). Molecular recognition between these two RNA modules has been shown to be critical for replication of the replicon (You et al. 2004; Friebe et al. 2005). The internal loop of 5BSL3.2 contains 6 nt which would hybridize with a sequence centered on
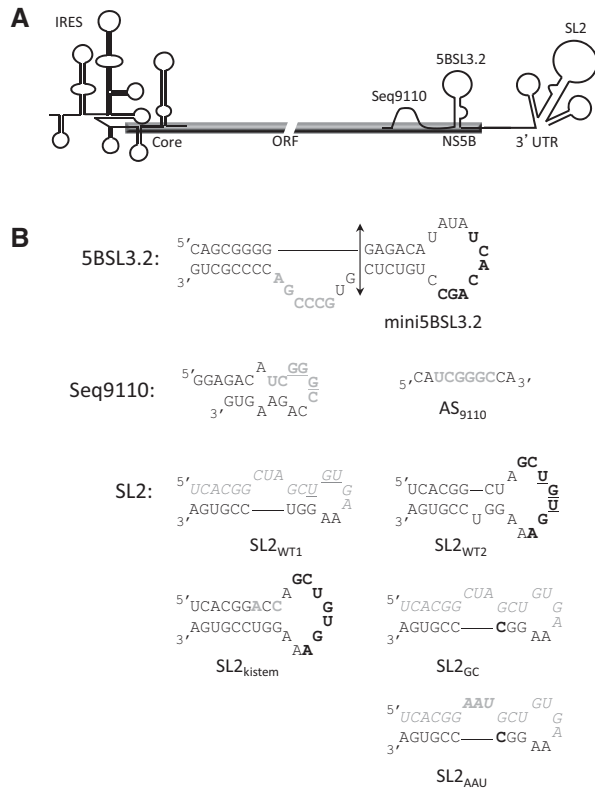
FIGURE 1. (*A*) Scheme of the HCV genome. The internal ribosome entry site (IRES) is on the 5′ side. The SL2 stem–loop is located in the 3′ UTR region. Seq9110 and 5BSL3.2 are located in the region coding for the NS5B protein. The region coding for the core protein (Core) is also shown. (*B*) Sequences and secondary structures of the RNAs. 5BSL3.2 was modified with a biotin tag at the 3′ end, allowing immobilization by streptavidin-biotin coupling on the sensor chips. The sequence in bold black indicates bases that could form Watson-Crick base pairs with SL2 (also in bold black). The sequence in bold gray indicates bases that could interact with Seq9110 or AS_{9110} (also in bold gray). Mini5BSL3.2 is a truncated version (double arrow) of 5BSL3.2 corresponding to the perfect stem–loop above the internal loop. AS_{9110} is an antisense oligonucleotide derivatized from Seq9110. For SL2, the sequences in italic gray indicate the palindromic sequence of SL2. Underlined bases for SL2 and Seq9110 indicate nucleotides that were replaced to generate hairpins of decreased affinity for 5BSL3.2: UGU was replaced by ACA for SL2, and GGG by AAA for Seq9110. $SL2_{WT1}$ and $SL2_{WT2}$ are two predicted secondary structures of SL2 obtained from the Mfold web server (http://mfold.rna.albany.edu/?q=mfold/RNA-Folding-Form). Bases in bold gray for $SL2_{kistem}$ (A and C) indicate modifications that were made to convert $SL2_{WT2}$ in a perfect stem–loop structure. $SL2_{GC}$ was designed to generate a hairpin of increased stability compared with SL2 without altering the palindromic sequence. $SL2_{AAU}$ is a mutated version of $SL2_{GC}$ in which CUA was mutated in AAU (in bold gray).

nucleotide 9110 (referred to as Seq9110) (Fig. 1B; Diviney et al. 2008). This internal loop has also been implicated in a long-range RNA–RNA interaction with stem–loop IIId of the IRES (Romero-Lopez and Berzal-Herranz 2009), but there are conflicting results about the influence of this interaction on viral translation activity. It is hypothesized that 5BSL3.2 could act as a molecular switch depending on its in-

teraction with SL2 or Seq9110, therefore leading the viral genome toward translation, replication, or encapsidation (Tuplin et al. 2012).

Despite the role that these interactions are expected to play in the life cycle of the virus, they have not as yet been characterized by direct kinetic methods. Some of them could not even be observed when they were analyzed by NMR spectroscopy. We, therefore, wanted to address whether 5BSL3.2 and SL2 could, indeed, form a loop-loop complex, whether Seq9110 could interact with the internal loop of 5BSL3.2, and whether these interactions were mutually exclusive or not. For this purpose, we used surface plasmon resonance (SPR). This label-free technique can be used to assess the affinity and the kinetics of bimolecular (Morton and Myszka 1998) or even trimolecular complexes (Bernat et al. 2003; Walsh et al. 2003; Jomain et al. 2007; Di Primo 2008; Palau and Di Primo 2012). In some cases, stoichiometry can also be determined (Teulade-Fichou et al. 2003; Mistrik et al. 2004; Di Primo and Lebars 2007; Di Primo 2008). SPR is widely used to investigate protein–protein, protein–small molecules, or protein–DNA interactions (for review, see Rich and Myszka 2011) but rarely for investigating RNA–RNA complexes, likely due to their susceptibility to hydrolysis. In previous studies, we have successfully investigated interactions between RNA oligonucleotides with structured RNA of human viruses or cells (Ducongé et al. 2000; Aldaz-Carroll et al. 2002; Lebars et al. 2008; Dausse et al. 2011).

In this work, the imperfect stem–loop structure 5BSL3.2 was immobilized on a streptavidin-coated sensor chip. SL2 or Seq9110 RNA oligonucleotides were injected in a continuous flow of buffer. These interactions were characterized either in a bimolecular context with the 5BSL3.2-SL2 and 5BSL3.2-Seq9110 complexes or in a trimolecular context with the 5BSL3.2-SL2-Seq9110 ternary complex. In contrast with previous results obtained by NMR spectroscopy with the same short RNA sequences that we used in this work (Friebe et al. 2005) or SHAPE mapping with longer RNAs (Tuplin et al. 2012), we show that 5BSL3.2 can form a complex with SL2 through kissing-loop interactions. The internal loop of 5BSL3.2 is also able to hybridize with Seq9110. The kinetic analysis of the 5BSL3.2-SL2-Seq9110 ternary complex shows that the two bimolecular complexes 5BSL3.2-SL2 and 5BSL3.2-Seq9110 are not mutually exclusive. The two interactions can coexist, strongly suggesting that the two binding sites of 5BSL3.2, the apical and the internal loop, are structurally independent. We also found that SPR signals that could not be fitted with a 1:1 model of interaction when SL2 was injected over 5BSL3.2 could only be explained by the structural heterogeneity in a solution of SL2. We demonstrate that this stem–loop is, indeed, a highly dynamic structure that alternates between at least two conformations: one is able to recognize 5BSL3.2 through kissing interactions, and the other one is able to self-associate. Both of these interactions occur in the absence of any added protein. This result suggests that the conformational dynamics of SL2 could

play a crucial role for controlling the destiny of the genomic RNA.

RESULTS

Design of the RNA molecules

The RNA molecules used for the SPR experiments were designed according to previously published work on HCV genotype 1b (isolate Con1) (You et al. 2004; Friebe et al. 2005; You and Rice 2008). Located within the NS5B coding region, 5BSL3.2 folds as an imperfect hairpin displaying an apical and an internal loop (Fig. 1B) and has been shown to be crucial for replication. The predicted structure by the mfold server (Zuker 2003) was confirmed by NMR spectroscopy (Friebe et al. 2005). 5BSL3.2 was modified with a biotin tag at its 3′ end to allow immobilization on a streptavidin-coated sensor chip. SL2 was also designed according to the known secondary structure determined within the 3′X of HCV (Friebe and Bartenschlager 2002; Yi and Lemon 2003). This stem–loop was referred to as SL2 wild type (SL2$_{WT}$). The mfold server predicted three secondary structures for SL2. Only those that displayed the sequence for recognizing 5BSL3.2, partially (SL2$_{WT1}$, $\Delta G_{37°C} = -8.20$ kcal/mol) or entirely (SL2$_{WT2}$, $\Delta G_{37°C} = -7.60$ kcal/mol) in an apical loop are reported in Figure 1B. SL2 has been previously characterized by NMR spectroscopy (Friebe et al. 2005). In this work, the authors used 1.4 mM of RNA prepared either in 20 mM NaCl-5 mM acetic buffer, pH 5.5, or in 20 mM NaCl-20 mM phosphate buffer, pH 7. In these experimental conditions, only conformation SL2$_{WT2}$ was observed in solution. Seq9110 (Fig. 1B) was designed as a 21-nt-long RNA displaying the sequence that potentially recognizes the internal loop of 5BSL3.2 at a central position. The mfold server predicted one secondary structure (Fig. 1B) with an initial $\Delta G_{37°C}$ close to zero (-0.9 kcal/mol). The region encompassing nucleotide 9110 is supposedly unstructured (Diviney et al. 2008). To check whether or not a structured context was crucial for recognition, an antisense oligonucleotide was also designed, AS$_{9110}$ (Fig. 1B). This oligonucleotide contained the 6-nt recognition sequence and was flanked by CA nucleotides that are not expected to contribute to binding, in order to increase the SPR signal by increasing its molecular weight. As expected, no structure could be predicted by mfold.

Binding of SL2 and Seq9110 to 5BSL3.2

The results obtained when SL2$_{WT}$ was injected over the 5BSL3.2 functionalized surface are reported in Figure 2A. These experiments were performed using the SCK method, as described in Materials and Methods, which is faster than the classical method and avoids repeated steps of injection/regeneration that could alter the surface and the immobilized target. Binding is observed when SL2$_{WT}$ is injected at increasing concentrations. Flat sensorgrams were obtained when a mutated stem–loop in which UGU (underlined in Fig. 1B) was replaced by ACA was injected (SL2$_{aca}$) (Fig. 2A). This strongly confirms that the interaction between 5BSL3.2 and SL2$_{WT}$ can occur through kissing interactions between the sequences that have been previously proposed (Lee et al. 2004; You et al. 2004; Friebe et al. 2005). Interestingly, the sensorgrams (Fig. 2A) are not monophasic. When the results are
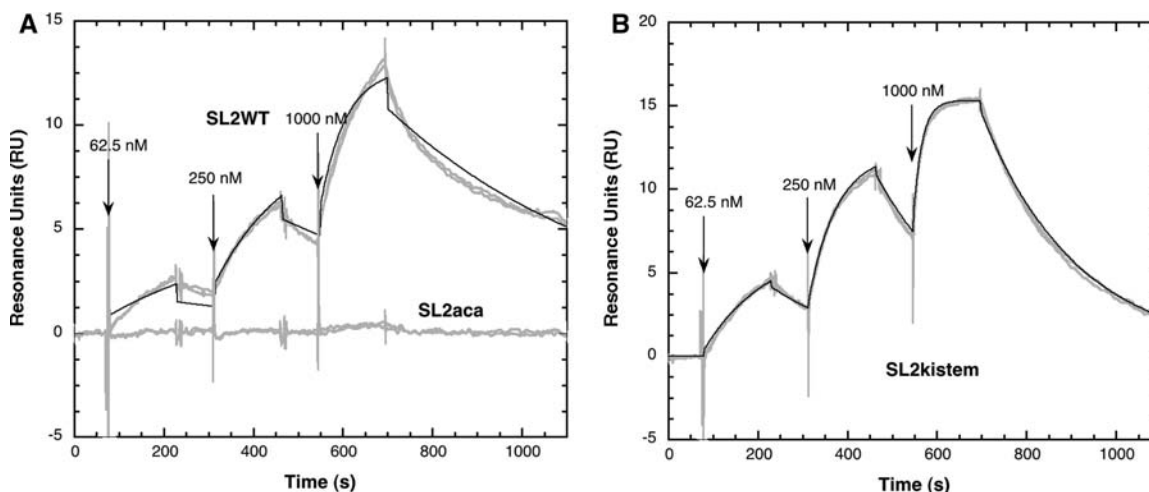

FIGURE 2. Kinetic analysis by the SCK method of SL2 hairpins binding to 5BSL3.2. The experiments were performed at 10°C on a SAHC200m sensor chip, at a flow rate of 50 μL/min. Thirty to 70 RU of biotinylated 5BSL3.2 were immobilized on the sensor chip. The samples were injected sequentially in the order of increasing concentrations, 62.5 nM (first arrow from the *left*), 250 nM (second arrow), and 1000 nM (third arrow). The regeneration was achieved with a 2-min pulse of a mixture of 40% formamide, 3.6 M urea, and 30 mM EDTA prepared in milli-Q water. The gray curves represent the experimental data (two overlaid sensorgrams). The black line represents the fit of one sensorgram to a Langmuir 1:1 model according to Equations (1) and (2) reported in the Supplemental Material. (*A*) SL2 wild type (SL2$_{WT}$) and the mutated SL2 stem–loop (SL2aca) in which the central UGU sequence of the loop was replaced by ACA. (*B*) SL2$_{kistem}$.

fitted with a simple Langmuir 1:1 model, there is a clear discrepancy between the data and the model used to fit them. Instead of trying to analyze the data with a more complicated model assuming, for instance, a conformational change after binding, a popular model often used to fit complex signals, we hypothesized that the nonmonophasic shape of the sensorgrams was simply due to a structural heterogeneity of $SL2_{WT}$.

We then analyzed $SL2_{WT}$ RNA using native gel electrophoresis in buffer conditions similar to those used for the SPR experiments, in particular, in the presence of 3 mM magnesium cations, in order to determine whether several structures do exist in solution (alternative monomeric structures, dimers) (Fig. 3). Strikingly, in contrast with previous results obtained by NMR spectroscopy suggesting that SL2 adopts only one conformation in solution, several bands and a smear are observed for $SL2_{WT}$, in the presence of Mg^{2+} and at much lower concentration of RNA (45 μM for the loaded sample instead of >1 mM for the NMR assays). This indicates that $SL2_{WT}$ may rapidly alternate between several structures, monomers (lower bands), and dimers (upper bands). The hypothesis that the unusual sensorgrams could be due to the heterogeneity of the 5BSL3.2 oligonucleotide was discarded because a single migrating band was visualized after loading of 5BSL3.2 on a native acrylamide gel (Supplemental Fig. S1).

We then hypothesized that mutations of $SL2_{WT}$ that would generate a perfect hairpin displaying in its apical loop the sequence for recognizing 5BSL3.2 by loop-loop interactions should result in one single band on the native gel, and the sensorgrams might be fitted with a 1:1 model. For this purpose, two modifications were made on the $SL2_{WT2}$ conformation (Fig. 1B). First, an adenine was added to generate an AU Watson-Crick pair with the unpaired U in the wild-type conformation ($SL2_{WT2}$), and the UG pair in the stem next to the loop was changed to CG. The mfold web server predicted one unique stem–loop structure ($\Delta G_{37°C} = -14.80$ kcal/mol), referred to as $SL2_{kistem}$ in Figure 1B. One single mi-

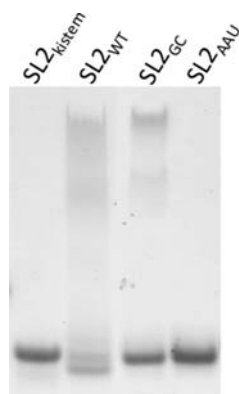**FIGURE 3.** Native acrylamide gels of SL2 hairpins. Two μg of $SL2_{WT}$, $SL2_{kistem}$, $SL2_{GC}$, and $SL2_{AAU}$ were prepared and were loaded on 15% (w/v) 75:1 acrylamide/bis(acrylamide) native gels as described in Materials and Methods. The gels were stained by "Stains-all."

grating band was observed when $SL2_{kistem}$ was loaded on a native gel (Fig. 3), and the sensorgrams were perfectly fitted with a Langmuir 1:1 model (Fig. 2B). The rate and the dissociation equilibrium constants for the 5BSL3.2-$SL2_{kistem}$ kissing complex are reported in Supplemental Table S1. In this work, only $SL2_{kistem}$ will be used for further analyses with 5BSL3.2.

We then investigated the interaction between 5BSL3.2 and Seq9110. In the preliminary experiments, RNA–RNA binding was characterized using the SCK method (Supplemental Fig. S2). Clear interaction was observed with slow association and dissociation phases. However, attempts to fit the sensorgrams with a Langmuir 1:1 model were not conclusive. The curve fittings clearly deviated from the sensorgrams, in particular, for the association phases. The experiments were repeated using the classical SPR method to analyze carefully the association phases on longer time scales (Fig. 4A). In these experiments, three concentrations of Seq9110 were injected in duplicate. The regeneration step was performed at least 800 sec after the beginning of the dissociation phase. Either at low, 250 nM, or high concentrations, 5 μM, duplicate overlaid sensorgrams demonstrated that regeneration was efficient. Again, the data still did not fit to a 1:1 model. Other attempts consisting of lowering the level of immobilization of biotinylated 5BSL3.2 to exclude problems related to a too high density of the immobilized target did not improve the curve fitting (data not shown). Seq9110 was loaded on a native gel to test a potential structural heterogeneity responsible for these findings. Seq9110 is slightly heterogeneous compared to the immobilized target 5BSL3.2 (Supplemental Fig. S1) but to a lesser extent than $SL2_{WT}$ (Fig. 3). We actually cannot conclude if this is a reason good enough to explain why these data could not be fitted with a 1:1 model. Despite the problems in determining the corresponding rate constants, the observed kinetics are clearly slower than those obtained with $SL2_{kistem}$. In addition, the results show that the interaction between the internal loop of 5BSL3.2 and Seq9110 is specific. Indeed, substitution of the three guanines by three adenines (Seq9110aaa) in the recognition sequence of Seq9110 (Fig. 1B) drastically decreases the binding (Supplemental Fig. S3).

An antisense oligonucleotide, AS_{9110} (Fig. 1B), was then injected over the immobilized 5BSL3.2 stem–loop (Fig. 4B) in order to investigate whether the 6-nt recognition sequence of Seq9110 required a secondary structure context to hybridize with the internal loop of 5BSL3.2. Clear binding was observed, but again, the data could not be fitted with a 1:1 model of interaction.

Since 5BSL3.2 has two binding sites for recognizing other RNA sequences of the HCV genome, the next step was to investigate the effect of the 5BSL3.2-SL2 interaction on 5BSL3.2-Seq9110 binding and whether these interactions were simultaneous or mutually exclusive. The experiments were performed by the single cycle kinetics on a decaying surface (SCKODS) method that was developed to analyze
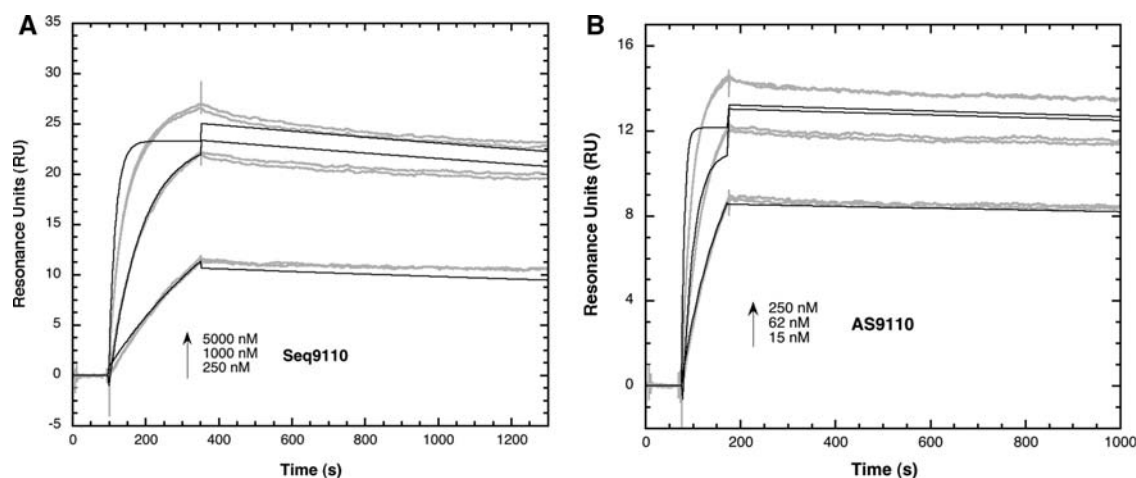
FIGURE 4. Kinetic analysis of Seq9110 and AS_{9110} binding to 5BSL3.2. The sensor chip was prepared as described in Figure 2 and in the Materials and Methods. RNA samples were injected over the functionalized surface in duplicate. Two overlaid sensorgrams (gray curves) are shown for each injected concentration. The regeneration of the surface was achieved with a 2-min pulse of a mixture of 40% formamide, 3.6 M urea, and 30 mM EDTA prepared in milli-Q water. The black lines represent the fit of one set of sensorgrams by global fitting analysis to a Langmuir 1:1 model. (*A*) Injection of Seq9110. (*B*) Injection of AS9110.

ternary complexes (Fig. 5; Palau and Di Primo 2012). Seq9110 was first injected over the biotinylated 5BSL3.2 target, immobilized on the streptavidin sensor chip. Then, while Seq9110 slowly dissociated from 5BSL3.2, the perfect stem–loop $SL2_{kistem}$ was injected sequentially in the order of increasing concentrations (Fig. 5). The sensorgrams are similar to those obtained when $SL2_{kistem}$ was injected on 5BSL3.2 in a bimolecular context, i.e., in the absence of Seq9110 (Fig. 2B). The rate and dissociation equilibrium constants determined by direct fitting of the sensorgrams are similar to those obtained when $SL2_{kistem}$ was injected in the absence of Seq9110 (Supplemental Table S1). No binding was observed when SL2aca was injected (Supplemental Fig. S4), in agreement with previous results (Fig. 2A). The results indicate that the two binding sites of 5BSL3.2 (apical and the internal loops) are structurally independent of each other. The reverse experiment confirms this finding. Saturation of the apical loop of 5BSL3.2 by SL2 did not prevent recognition between Seq9110 and the internal loop of the immobilized target (Supplemental Fig. S5).

Self-association of SL2

Previous works suggested that SL2 could be responsible for the dimerization of the viral RNA (Ivanyi-Nagy et al. 2006; Shetty et al. 2010). The results obtained with SL2 also prompted us to further investigate this stem–loop structure that displays a palindromic sequence. A new $SL2_{WT}$ was synthesized with a biotin at its 5′ end. It was immobilized on a streptavidin-coated sensor chip. First, we checked that this new target could recognize a version of 5BSL3.2 shortened above its internal loop (Fig. 1B). The result is reported in Figure 6. Then, $SL2_{WT}$ and other SL2 nonbiotinylated hair-

pins were injected over the immobilized stem–loop $SL2_{WT}$ (Fig. 6). The results clearly show that $SL2_{WT}$ is able to interact with itself. In contrast, $SL2_{kistem}$, designed to generate a stable conformation with an apical loop exhibiting the recognition sequence for kissing 5BSL3.2, was not able to bind to biotinylated $SL2_{WT}$. Replacement of the GU pair next to the bulge of conformation $SL2_{WT1}$ (Fig. 1B) by a GC pair ($SL2_{GC}$) led to decreased binding, suggesting that increased stability of the 3-nt stem was unfavorable for self-association. This result was confirmed when $SL2_{GC}$ was loaded on a native gel (Fig. 3). The migration pattern of $SL2_{GC}$ resembles that of $SL2_{WT}$, indicating that this stem–loop structure can still dimerize, but the lower bands are favored suggesting that the conformational equilibrium is shifted toward monomers. $SL2_{GC}$ behaved kinetically as $SL2_{WT}$ does for binding to 5BSL3.2: the sensorgrams were not monophasic (Supplemental Fig. S6A), which is consistent with the structural heterogeneity of $SL2_{GC}$. Binding was abolished when, in addition, the CUA bulge was mutated to AAU (Fig. 6). In this case, one single band was observed on the native gel (Fig. 3), demonstrating that the bulge of SL2 was crucial for dimerization. Attempts to fit these data to a 1:1 model were not successful, likely due again to the structural heterogeneity of the $SL2_{WT}$ RNA immobilized on the sensor chip surface (Supplemental Fig. S6B–D).

DISCUSSION

We investigated RNA–RNA interactions at the 3′ end of the HCV genome by SPR. This technique is a valuable tool for investigating molecular interactions in real time at a solid-liquid interface. However, it can be challenging when working with molecules such as RNA that are prone to hydrolysis,
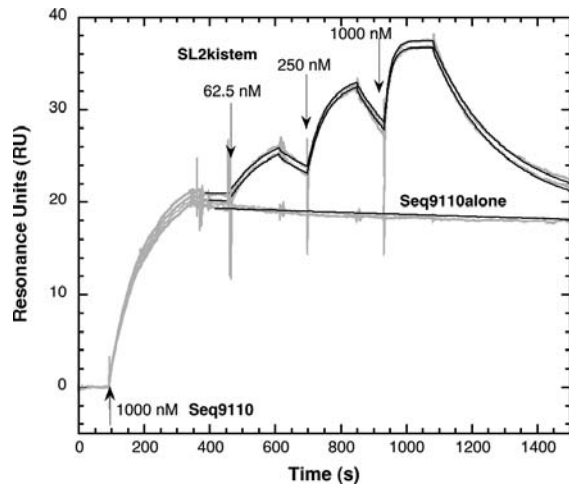
FIGURE 5. Kinetic analysis by the SCKODS method of SL2$_{kistem}$ hairpin and Seq9110 binding to 5BSL3.2. The sensor chip was prepared as described in Figure 2 and in Materials and Methods. Seq9110 was first injected over the 5BSL3.2-coated surface at 1 µM (first arrow from the *left*). During the dissociation phase of the formed Seq9110-5BSL3.2 complex, SL2$_{kistem}$ was injected sequentially in the order of increasing concentrations, 62.5 nM (second arrow), 250 nM (third arrow), and 1000 nM (fourth arrow). Experiments were performed with injections of Seq9110 only (referred to as Seq9110 alone). The regeneration of the surface was achieved with a 2-min pulse of a mixture of 40% formamide, 3.6 M urea, and 30 mM EDTA prepared in milli-Q water. The gray curves represent the experimental data (two overlaid sensorgrams for SL2$_{kistem}$ and Seq9110 alone). The black line for Seq9110 alone represents the fit of the dissociation phase according to Equation (2). The black lines for SL2$_{kistem}$ represent the fit to a Langmuir 1:1 model of interaction according to Equations (1) and (2) by the SCKODS method.

in particular, in buffer containing magnesium ions. We have developed protocols that allow users to investigate complexes with short RNA sequences without encountering any major problems regarding the integrity of the RNA immobilized on the sensor chip surface (Di Primo et al. 2011).

Despite previous data showing the central role of 5BSL3.2 in the life cycle of the virus by long-range RNA–RNA interaction with other genomic sequences such as SL2 (Friebe et al. 2005; Murayama et al. 2010; Schmitt et al. 2011) and the region centered on nucleotide 9110 (Diviney et al. 2008), surprisingly, there were no data obtained by kinetic methods demonstrating direct interaction between these RNA motifs. NMR spectroscopy has been used to characterize SL2 and 5BSL3.2 (Friebe et al. 2005), but the kissing complex potentially formed between these two imperfect hairpins could not be observed. Surface plasmon resonance-based instruments provide real-time monitoring of virtually all kinds of complexes since the signal results from mass changes upon binding of an injected partner over a target-functionalized sensor chip surface. An interesting feature of some of these instruments resides in that the experiments can be performed at any temperature between 4°C and 45°C. This can be used either to stabilize or to destabilize complexes that could be difficult to characterize at room temperature (23°C). During the

preliminary experiments with SL2, we noticed that the rate of dissociation was very fast. We then decided to monitor the interactions at a temperature low enough (10°C) to slow down the dissociation phase.

Our results clearly demonstrate that SL2 recognizes 5BSL3.2 through kissing interactions. Interestingly, the corresponding sensorgrams showed nonmonophasic shapes. Adding one more step to the initial Langmuir 1:1 model interaction would have easily fitted the data because two exponentials mathematically fit better than one, three better than two, etc. A typical model describing a two-step reaction is based on a conformational change after binding. When the 1:1 model seems not to be appropriate, the two-step reaction model always fits the data better. The use of this model is subject to controversy and debate. The dogma is that SPR cannot detect conformational changes because the signal is due only to changes of mass at the solid–liquid interface. However, a few published works argued that only a conformational change after binding could explain unexpected signals obtained (Winzor 2003; Wood and Lee 2005; Christopeit et al. 2009; Dell'Orco et al. 2010). Before we considered using such a model of interaction, we hypothesized that the kinetic characteristics of SL2$_{WT}$ binding to 5BSL3.2 were due to structural heterogeneity of the RNA sample. This was clearly demonstrated after loading SL2$_{WT}$ on a native acrylamide gel. Noteworthy, we could stabilize one of the predicted conformations, SL2$_{WT2}$ (Fig. 1B), by pairing the unpaired U with an A and changing the UG pair next to the apical loop to a CG one. The SL2$_{WT2}$ conformation corresponds to that observed in solution by NMR spectroscopy (Friebe et al. 2005). The perfect hairpin that was generated from this conformation did follow a 1:1 model of interaction with 5BSL3.2. The exact
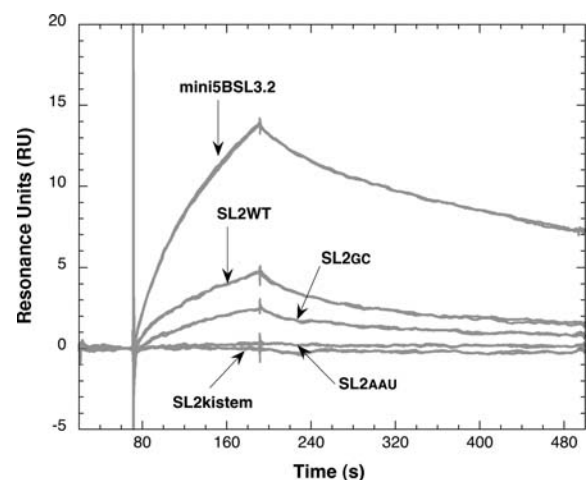

FIGURE 6. Kinetic analysis of SL2 binding to itself. SL2$_{WT}$ was biotinylated at its 5′ end and immobilized on a streptavidin-coated CM5 sensor chip. SL2 hairpins were injected in duplicate at 500 nM as indicated by the arrows. The experiments were performed at 10°C and at a flow rate of 50 µL/min. The truncated version of 5BSL3.2, mini5BSL3.2, was also injected over the SL2 functionalized surface.

origin of the multiphasic shape of the sensorgrams remains unclear (Fig. 2A). This would require further investigation to find which structures contribute to the signal and to what extent, or to analyze whether, in some cases, SPR is, indeed, able to monitor conformational changes after a binding step. In any case, the results point out that caution should be taken before analyzing SPR data with kinetic models of more than a one-step reaction when complexity is just due to structural heterogeneity of the samples. This is obviously of relevance when working with RNAs.

Our data confirm previous hypotheses that suggested a kissing complex between 5BSL3.2 and SL2, but they do not agree with the results from NMR analysis (Friebe et al. 2005) or SHAPE mapping on the HCV genotype 1b (isolate Con1) (Tuplin et al. 2012). No interaction was detected by NMR assays with the same short RNA sequences that we used, and a unique secondary structure was proposed for SL2. We did not find a unique structure for the unmodified SL2. Our results demonstrate that SL2 fluctuates between at least two conformations: $SL2_{WT1}$ and $SL2_{WT2}$ (Fig. 1B). In the SHAPE study on the Con1 isolate, Tuplin et al. found that SL2 resembled the structure determined by NMR ($SL2_{WT2}$) (Fig. 1B) and that the SL2-5BSL3.2 loop–loop complex was largely absent. They concluded that the adoption of the known stem–loop SL2 conformation ($SL2_{WT2}$) (Fig. 1B) was incompatible with kissing-complex formation (Tuplin et al. 2012). This conclusion is somehow surprising. Previous works have shown that stable kissing complexes can only be formed through Watson-Crick base-pairing between the partially or totally complementary sequences of apical loops, i.e., in a stem–loop context (Westhof et al. 1988; Lee and Crothers 1998; Mujeeb et al. 1998; Kim and Tinoco 2000; Ennifar et al. 2001; Lebars et al. 2008; Van Melckebeke et al. 2008). The intermolecular loop–loop helix is stacked between the two stem helices. We observed direct interaction between the unmodified SL2 and 5BSL3.2, two RNA oligonucleotides similar to those used by Friebe et al. (2005). Furthermore, an interaction was observed that followed a perfect 1:1 model when SL2 was mutated to generate a perfect hairpin that displayed the proposed kissing sequence in its apical loop ($SL2_{kistem}$) (Fig. 1B).

It is not at all clear why the NMR and SPR experiments did not agree even when the same RNA sequences were investigated. The NMR assays were performed at 5°C and 25°C. The SPR experiments were performed at 10°C. Temperature is unlikely to be the reason for this discrepancy. One difference between the SPR experiments and the NMR analysis is that our assays were carried out in the presence of magnesium ions. The role of magnesium ions in the stability and structure of RNA is well-known. The stabilizing role of magnesium ions in natural or artificial kissing complexes has been characterized (Eguchi and Tomizawa 1991; Gregorian and Crothers 1995; Ducongé et al. 2000). One magnesium ion would bind at the center of a pocket made by the two phosphate clusters at the stem–loop junctions (Chang and Tinoco 1997; Lee and Crothers 1998; Jossinet et al. 1999; Reblova et al. 2003). In theory, the high concentration of RNA used for the NMR experiments (1.2–1.4 mM) should have compensated for the absence of magnesium, since the stability of bimolecular nucleic acid–nucleic acid complexes depends on the total concentration (Puglisi and Tinoco 1989).

The results confirm that the sequence centered on nucleotide 9110 can recognize the internal loop of 5BSL3.2. Binding can also occur with an antisense sequence of the internal loop of 5BSL3.2, supporting previous findings that suggested that the sequence centered on nucleotide 9110 was likely unstructured (Diviney et al. 2008). Together, these results support a view in which recognition between the internal loop of 5BSL3.2 and the sequence centered on nucleotide 9110 would not require structured motifs to occur, in contrast to what has been proposed recently (Shetty et al. 2013). The results raise the problem of the kinetics of formation of these complexes. We do not understand why data obtained with the same immobilized target but with different partners cannot be fitted with a 1:1 model of interaction. This problem is further discussed in the Supplemental Material (Supplemental Fig. S7).

Our work demonstrates that SL2 and Seq9110 motifs do not compete for binding to 5BSL3.2. SL2 behaved similarly in the presence or in the absence of Seq9110, suggesting that the apical and internal loops are two structurally independent modules for interacting. These results, obtained with short RNA sequences, are in good agreement with a recent work with longer RNAs analyzed by SHAPE mapping that suggested that these interactions could occur simultaneously (Tuplin et al. 2012). Together, they strongly support previous works suggesting that 5BSL3.2 could be involved in a complex pseudoknot, implicating nonexclusive, long-range interactions between the internal loop of 5BSL3.2 and the sequence centered on nucleotide 9110 and between the apical loop of 5BSL3.2 and SL2 (Diviney et al. 2008; Shetty et al. 2013).

The structural heterogeneity of SL2 observed on native acrylamide gels and the self-association measured by SPR strongly suggests that SL2 can dimerize. Dimerization of viral genomes is normally a unique property of retroviruses involving interaction with the nucleocapsid and has been extensively documented (Paillart et al. 1996, 2004; Lu et al. 2011). As far as HCV is concerned, previous works have shown that SL2 displays a palindromic sequence, named dimer linkage sequence (DLS) (Cristofari et al. 2004; Ivanyi-Nagy et al. 2006), which spans from the 5′-terminal uracile to the first adenine nucleotide in the apical loop of the $SL2_{WT1}$ conformation (Fig. 1B). Present in the 3′X between stem–loop SL1 and SL3, this sequence would mediate the dimerization of the 3′ UTR in the presence of the core protein of HCV (Cristofari et al. 2004; Ivanyi-Nagy et al. 2006; Sharma et al. 2012). In another work, the authors showed that the RNA dimerization would be mediated via a kissing complex intermediate between two structurally rearranged DLS. The core protein would then stabilize the resulting extended duplex

(Shetty et al. 2010). Our results show that the minimal structured motif of the 3′ UTR containing the dimer linkage sequence SL2 is able to dimerize in vitro in the absence of any added protein. The results obtained with SL2$_{kistem}$ and SL2$_{AAU}$ bring strong experimental evidence that the upper bands observed in the native gel are, indeed, dimers (Fig. 3). Upper bands are not observed if the sequence that triggers the dimerization is locked in a perfect stem–loop structure (SL2$_{kistem}$) that is too stable to allow structural rearrangements or if this sequence is mutated (SL2$_{AAU}$). The biological role of the dimerization process is still subject to debate. It is commonly believed that the HCV virion contains a single copy of the genomic RNA, but to our knowledge, this has not as yet been formally established.

We have investigated by SPR the interactions between RNA motifs at the 3′ end of the HCV genotype 1b (isolate Con1). We conclude that the kissing complex formed by SL2 and 5BSL3.2, which was not observed by NMR analysis with the same short RNA sequences that we used or was largely absent when investigated by SHAPE mapping with longer RNAs, is compatible with the SL2$_{WT2}$ conformation of SL2. This bimolecular interaction does not prevent binding of the sequence centered on nucleotide 9110. The two binding sequences, the apical and internal loops of 5BSL3.2, are structurally independent. The two interactions can coexist. We show that SL2 exists in a conformational equilibrium between at least two conformations: one that recognizes 5BSL3.2 through loop–loop interactions (SL2$_{WT2}$) (Fig. 1B) and the other one that allows self-association (SL2$_{WT1}$) (Fig. 1B). The SL2 region is, therefore, involved in two different interactions that are likely exclusive, leading consequently to different activities, translation, replication, or encapsidation during the viral replication, as also suggested by a work published recently during the review of our manuscript (Shetty et al. 2013).

MATERIALS AND METHODS

Oligonucleotides

RNA oligonucleotides, including those with a biotin tag at the 3′ or 5′ ends, were synthesized on an Expedite 8908 synthesizer (Applied Biosystems) or were purchased from Dharmacon (Fermentas). After deprotection following the manufacturer's instructions, the oligonucleotides were purified by electrophoresis on 7 M urea 20% polyacrylamide gels, electro-eluted, and desalted on Sephadex G-25 (GE Healthcare Lifesciences) spin columns prepared in 1-mL syringes. Pure samples in milli-Q water were assayed at 260 nm with a Nanodrop ND-1000 spectrophotometer (Labtech) to determine their concentration using extinction coefficients calculated at http://www.eurofinsdna.com/home.html. The samples were stored at −20°C. Before any experiment, the RNA oligogucleotides were diluted in the appropriate buffer and heated for 1 min, 30 sec at 90°C, then put on ice for 5 min. The predictions of the secondary structures were performed with the mfold web server at http://mfold.rna.albany.edu/?q=mfold/RNA-Folding-Form (Zuker 2003).

Native gels and staining of the RNA oligonucleotides

Native gels were prepared using 15% (w/v) 75:1 acrylamide/bis(acrylamide) in 50 mM Tris-acetate buffer, pH 7.3 at 20°C, containing 3 mM magnesium acetate (migration buffer). Two or 4 μg of RNA were diluted in the migration buffer, heated 1 min, 30 sec at 90°C, then put on ice for 5 min. The samples were loaded on the gel equilibrated at 4°C. The electrophoresis was carried out at 300 V for 5 h. The gels were stained for 30 min in the dark using the "Stains-all" dye (Acros Organics), then washed with distilled water and discolored in daylight.

Surface plasmon resonance experiments

The SPR experiments were performed at 10°C with a Biacore T200 apparatus (Biacore) using either SAHC200m sensor chips functionalized with streptavidin by the manufacturer (Xantec Bioanalytics) or CM5 sensor chips (Biacore). These surfaces were coated at the laboratory with 1000–1500 resonance units (RU) of streptavidin (Roche Applied Sciences) using the Biacore amine-coupling kit and HBS-EP running buffer (Biacore). Thirty to 70 RU of biotinylated RNA were immobilized on one flow cell of the sensor chip by injecting solutions prepared at 5–50 nM either in the HBS-EP buffer or in the running buffer used for the binding experiments (10 mM sodium phosphate buffer, pH 7.2 at 20°C, containing 50 mM sodium chloride, 3 mM magnesium chloride and 0.05% Tween-20). One flow cell left blank was used as a reference. All injected RNA samples were prepared in the running buffer. They were injected over the functionalized surface at 50 μL/min. The binding kinetics were monitored using the single cycle kinetics (SCK) method (Karlsson et al. 2006), in which the samples are injected sequentially in the order of increasing concentrations and the regeneration step is performed at the end of the cycle, by the single cycle kinetics on a decaying surface method (Palau and Di Primo 2012), in which the samples are injected sequentially in the order of increasing concentrations during a dissociation phase and the regeneration step is performed at the end of each cycle, or by the classical method in which the samples are injected one by one, with a regeneration step performed after each injection. The regeneration of the functionalized surface, the purpose of which is to remove any partner still interacting with the immobilized target after the dissociation phase, was achieved with a 2-min pulse of a mixture of 40% formamide, 3.6 M urea, and 30 mM EDTA prepared in milli-Q water. These conditions were mild enough so that the same functionalized sensor chip could be used for more than 50 cycles of injection/regeneration without major loss of the SPR signal. The sensorgrams, which correspond to the variation of the SPR signal expressed in resonance units (RU) as a function of time, were double-referenced (Myszka 1999) using BiaEval 4.1 (Biacore). This removes any contribution to the signal that may result from the RNA samples and the buffer flowing over the blank flow cell and the functionalized one, respectively.

The association and dissociation rate constant k_a and k_d, respectively, for the RNA–RNA complexes were determined by direct curve fitting of the sensorgrams assuming a Langmuir 1:1 model (see Supplemental Material for details). The dissociation equilibrium constant, K_D, was calculated as k_d/k_a.

SUPPLEMENTAL MATERIAL

Supplemental material is available for this article.

REFERENCES

Aldaz-Carroll L, Tallet B, Dausse E, Yurchenko L, Toulmé JJ. 2002. Apical loop–internal loop interactions: A new RNA–RNA recognition motif identified through in vitro selection against RNA hairpins of the hepatitis C virus mRNA. *Biochemistry* **41:** 5883–5893.

Bernat B, Pal G, Sun M, Kossiakoff AA. 2003. Determination of the energetics governing the regulatory step in growth hormone-induced receptor homodimerization. *Proc Natl Acad Sci* **100:** 952–957.

Chang KY, Tinoco I Jr. 1997. The structure of an RNA "kissing" hairpin complex of the HIV TAR hairpin loop and its complement. *J Mol Biol* **269:** 52–66.

Christopeit T, Gossas T, Danielson UH. 2009. Characterization of Ca²⁺ and phosphocholine interactions with C-reactive protein using a surface plasmon resonance biosensor. *Anal Biochem* **391:** 39–44.

Clarke B. 1997. Molecular virology of hepatitis C virus. *J Gen Virol* **78:** 2397–2410.

Cristofari G, Ivanyi-Nagy R, Gabus C, Boulant S, Lavergne JP, Penin F, Darlix JL. 2004. The hepatitis C virus Core protein is a potent nucleic acid chaperone that directs dimerization of the viral (+) strand RNA in vitro. *Nucleic Acids Res* **32:** 2623–2631.

Dausse E, Taouji S, Evadé L, Di Primo C, Chevet E, Toulmé JJ. 2011. HAPIscreen, a method for high-throughput aptamer identification. *J Nanobiotechnology* **9:** 25.

Dell'Orco D, Muller M, Koch KW. 2010. Quantitative detection of conformational transitions in a calcium sensor protein by surface plasmon resonance. *Chem Commun (Camb)* **46:** 7316–7318.

Di Primo C. 2008. Real time analysis of the RNAI–RNAII–Rop complex by surface plasmon resonance: From a decaying surface to a standard kinetic analysis. *J Mol Recognit* **21:** 37–45.

Di Primo C, Lebars I. 2007. Determination of refractive index increment ratios for protein–nucleic acid complexes by surface plasmon resonance. *Anal Biochem* **368:** 148–155.

Di Primo C, Dausse E, Toulmé JJ. 2011. Surface plasmon resonance investigation of RNA aptamer–RNA ligand interactions. *Methods Mol Biol* **764:** 279–300.

Diviney S, Tuplin A, Struthers M, Armstrong V, Elliott RM, Simmonds P, Evans DJ. 2008. A hepatitis C virus *cis*-acting replication element forms a long-range RNA-RNA interaction with upstream RNA sequences in NS5B. *J Virol* **82:** 9008–9022.

Ducongé F, Di Primo C, Toulmé JJ. 2000. Is a closing "GA pair" a rule for stable loop-loop RNA complexes? *J Biol Chem* **275:** 21287–21294.

Eguchi Y, Tomizawa J. 1991. Complexes formed by complementary RNA stem-loops: Their formations, structures and interaction with ColE1 Rom protein. *J Mol Biol* **220:** 831–842.

Ennifar E, Walter P, Ehresmann B, Ehresmann C, Dumas P. 2001. Crystal structures of coaxially stacked kissing complexes of the HIV-1 RNA dimerization initiation site. *Nat Struct Biol* **8:** 1064–1068.

Friebe P, Bartenschlager R. 2002. Genetic analysis of sequences in the 3′ nontranslated region of hepatitis C virus that are important for RNA replication. *J Virol* **76:** 5326–5338.

Friebe P, Boudet J, Simorre JP, Bartenschlager R. 2005. Kissing-loop interaction in the 3′ end of the hepatitis C virus genome essential for RNA replication. *J Virol* **79:** 380–392.

Gregorian RS Jr, Crothers DM. 1995. Determinants of RNA hairpin loop-loop complex stability. *J Mol Biol* **248:** 968–984.

Ivanyi-Nagy R, Kanevsky I, Gabus C, Lavergne JP, Ficheux D, Penin F, Fosse P, Darlix JL. 2006. Analysis of hepatitis C virus RNA dimerization and core-RNA interactions. *Nucleic Acids Res* **34:** 2618–2633.

Jomain JB, Tallet E, Broutin I, Hoos S, van Agthoven J, Ducruix A, Kelly PA, Kragelund BB, England P, Goffin V. 2007. Structural and thermodynamic bases for the design of pure prolactin receptor antagonists: X-ray structure of Del1–9-G129R-hPRL. *J Biol Chem* **282:** 33118–33131.

Jossinet F, Paillart JC, Westhof E, Hermann T, Skripkin E, Lodmell JS, Ehresmann C, Ehresmann B, Marquet R. 1999. Dimerization of HIV-1 genomic RNA of subtypes A and B: RNA loop structure and magnesium binding. *RNA* **5:** 1222–1234.

Karlsson R, Katsamba PS, Nordin H, Pol E, Myszka DG. 2006. Analyzing a kinetic titration series using affinity biosensors. *Anal Biochem* **349:** 136–147.

Kim CH, Tinoco I Jr. 2000. A retroviral RNA kissing complex containing only two G·C base pairs. *Proc Natl Acad Sci* **97:** 9396–9401.

Lebars I, Legrand P, Aimé A, Pinaud N, Fribourg S, Di Primo C. 2008. Exploring TAR–RNA aptamer loop–loop interaction by X-ray crystallography, UV spectroscopy and surface plasmon resonance. *Nucleic Acids Res* **36:** 7146–7156.

Lee AJ, Crothers DM. 1998. The solution structure of an RNA loop–loop complex: The *ColE1* inverted loop sequence. *Structure* **6:** 993–1005.

Lee H, Shin H, Wimmer E, Paul AV. 2004. *cis*-acting RNA signals in the NS5B C-terminal coding sequence of the hepatitis C virus genome. *J Virol* **78:** 10865–10877.

Lu K, Heng X, Summers MF. 2011. Structural determinants and mechanism of HIV-1 genome packaging. *J Mol Biol* **410:** 609–633.

Mistrik P, Moreau F, Allen JM. 2004. BiaCore analysis of leptin–leptin receptor interaction: Evidence for 1:1 stoichiometry. *Anal Biochem* **327:** 271–277.

Morton TA, Myszka DG. 1998. Kinetic analysis of macromolecular interactions using surface plasmon resonance biosensors. *Methods Enzymol* **295:** 268–294.

Mujeeb A, Clever JL, Billeci TM, James TL, Parslow TG. 1998. Structure of the dimer initiation complex of HIV-1 genomic RNA. *Nat Struct Biol* **5:** 432–436.

Murayama A, Weng L, Date T, Akazawa D, Tian X, Suzuki T, Kato T, Tanaka Y, Mizokami M, Wakita T, et al. 2010. RNA polymerase activity and specific RNA structure are required for efficient HCV replication in cultured cells. *PLoS Pathog* **6:** e1000885.

Myszka DG. 1999. Improving biosensor analysis. *J Mol Recognit* **12:** 279–284.

Paillart JC, Marquet R, Skripkin E, Ehresmann C, Ehresmann B. 1996. Dimerization of retroviral genomic RNAs: Structural and functional implications. *Biochimie* **78:** 639–653.

Paillart JC, Shehu-Xhilaga M, Marquet R, Mak J. 2004. Dimerization of retroviral RNA genomes: An inseparable pair. *Nat Rev Microbiol* **2:** 461–472.

Palau W, Di Primo C. 2012. Single-cycle kinetic analysis of ternary DNA complexes by surface plasmon resonance on a decaying surface. *Biochimie* **94:** 1891–1899.

Puglisi JD, Tinoco I Jr. 1989. Absorbance melting curves of RNA. *Methods Enzymol* **180:** 304–325.

Reblova K, Spackova N, Sponer JE, Koca J, Sponer J. 2003. Molecular dynamics simulations of RNA kissing-loop motifs reveal structural dynamics and formation of cation-binding pockets. *Nucleic Acids Res* **31:** 6942–6952.

Rich RL, Myszka DG. 2011. Survey of the 2009 commercial optical biosensor literature. *J Mol Recognit* **24:** 892–914.

Romero-Lopez C, Berzal-Herranz A. 2009. A long-range RNA–RNA interaction between the 5′ and 3′ ends of the HCV genome. *RNA* **15:** 1740–1752.

Schmitt M, Scrima N, Radujkovic D, Caillet-Saguy C, Simister PC, Friebe P, Wicht O, Klein R, Bartenschlager R, Lohmann V, et al. 2011. A comprehensive structure-function comparison of hepatitis C virus strain JFH1 and J6 polymerases reveals a key residue stimulating replication in cell culture across genotypes. *J Virol* **85:** 2565–2581.

Sharma KK, de Rocquigny H, Darlix JL, Lavergne JP, Penin F, Lessinger JM, Mely Y. 2012. Analysis of the RNA chaperoning activity of the hepatitis C virus core protein on the conserved 3′X region of the viral genome. *Nucleic Acids Res* **40:** 2540–2553.

Shetty S, Kim S, Shimakami T, Lemon SM, Mihailescu MR. 2010. Hepatitis C virus genomic RNA dimerization is mediated via a kissing complex intermediate. *RNA* **16:** 913–925.

Shetty S, Stefanovic S, Mihailescu MR. 2013. Hepatitis C virus RNA: Molecular switches mediated by long-range RNA–RNA interactions? *Nucleic Acids Res* **41:** 2526–2540.

Tanaka T, Kato N, Cho MJ, Shimotohno K. 1995. A novel sequence found at the 3′ terminus of hepatitis C virus genome. *Biochem Biophys Res Commun* **215:** 744–749.

Teulade-Fichou MP, Carrasco C, Guittat L, Bailly C, Alberti P, Mergny JL, David A, Lehn JM, Wilson WD. 2003. Selective recognition of G-quadruplex telomeric DNA by a bis(quinacridine) macrocycle. *J Am Chem Soc* **125:** 4732–4740.

Tuplin A, Struthers M, Simmonds P, Evans DJ. 2012. A twist in the tail: SHAPE mapping of long-range interactions and structural rearrangements of RNA elements involved in HCV replication. *Nucleic Acids Res* **40:** 6908–6921.

Van Melckebeke H, Devany M, Di Primo C, Beaurain F, Toulmé JJ, Bryce DL, Boisbouvier J. 2008. Liquid-crystal NMR structure of HIV TAR RNA bound to its SELEX RNA aptamer reveals the origins of the high stability of the complex. *Proc Natl Acad Sci* **105:** 9210–9215.

Walsh ST, Jevitts LM, Sylvester JE, Kossiakoff AA. 2003. Site2 binding energetics of the regulatory step of growth hormone–induced receptor homodimerization. *Protein Sci* **12:** 1960–1970.

Westhof E, Dumas P, Moras D. 1988. Restrained refinement of two crystalline forms of yeast aspartic acid and phenylalanine transfer RNA crystals. *Acta Crystallogr A* **44:** 112–123.

Winzor DJ. 2003. Surface plasmon resonance as a probe of protein isomerization. *Anal Biochem* **318:** 1–12.

Wood DO, Lee JS. 2005. Investigation of pH-dependent DNA–metal ion interactions by surface plasmon resonance. *J Inorg Biochem* **99:** 566–574.

Yi M, Lemon SM. 2003. 3′ nontranslated RNA signals required for replication of hepatitis C virus RNA. *J Virol* **77:** 3557–3568.

You S, Rice CM. 2008. 3′ RNA elements in hepatitis C virus replication: Kissing partners and long poly(U). *J Virol* **82:** 184–195.

You S, Stump DD, Branch AD, Rice CM. 2004. A *cis*-acting replication element in the sequence encoding the NS5B RNA-dependent RNA polymerase is required for hepatitis C virus RNA replication. *J Virol* **78:** 1352–1366.

Zuker M. 2003. Mfold web server for nucleic acid folding and hybridization prediction. *Nucleic Acids Res* **31:** 3406–3415.